EFDA–JET–PR(10)20

C. Perez von Thun, A. Perona, T. Johnson, S.E. Sharapov, M. Reich, V.G. Kiptily, M. Cecconello, A. Salmi, V. Ya. Goloborod'ko, S.D. Pinches, M. García-Muñoz, D. Darrow, M. Brix, I. Voitsekhovitch and JET EFDA contributors

Numerical Simulation of Scintillation Detector Measurements for Fast Ion Losses Induced by Fishbones on JET

Numerical Simulation of Scintillation Detector Measurements for Fast Ion Losses Induced by Fishbones on JET

C. Perez von Thun[1], A. Perona[2], T. Johnson[3], S.E. Sharapov[4], M. Reich[1], V.G. Kiptily[4], M. Cecconello[5], A. Salmi[6], V. Ya. Goloborod'ko[7], S.D. Pinches[4], M. García-Muñoz[1], D. Darrow[8], M. Brix[4], I. Voitsekhovitch[4] and JET EFDA contributors*

JET-EFDA, Culham Science Centre, OX14 3DB, Abingdon, UK

[1]Max-Planck-Institut f¨ur Plasmaphysik, EURATOM-Association IPP, Garching, D-85748, Germany
[2]Burning Plasma Research Group, Politecnico di Torino, 10129 Torino, Italy
[3]EURATOM-VR Association, Fusion Plasma Physics, EES, KTH, 10044 Stockholm, Sweden
[4]EURATOM-CCFE Fusion Association, Culham Science Centre, OX14 3DB, Abingdon, OXON, UK
[5]EURATOM-VR Association, Department of Physics and Astronomy, Uppsala University, 75120 Uppsala, Sweden
[6]Helsinki University of Technology, Association EURATOM-Tekes, Finland
[7]Association EURATOM/OEAW, Institute for Theoretical Physics, University of Innsbruck, Austria
[8]Princeton Plasma Physics Laboratory, Princeton, New Jersey
** See annex of F. Romanelli et al, "Overview of JET Results",*
(Proc. 22[nd] IAEA Fusion Energy Conference, Geneva, Switzerland (2008)).

Preprint of Paper to be submitted for publication in
Nuclear Fusion

ABSTRACT

A synthetic diagnostic model for the simulation of energy and pitch angle resolved measurements of fast ion losses obtained by 2D scintillation-type detectors is presented and subsequently tested on a JET discharge with fishbones (previously documented in [Perez von Thun C *et al Nucl. Fusion* **50** (2010) 084009]). The simulated energy and pitch angle distributions at the detector are found to be in excellent agreement with the measurements.

INTRODUCTION

To achieve ignition (or high Q-values) in a D-T operated magnetic confinement fusion device and prevent damage to plasma facing wall elements [1], it is necessary that the fast (i.e. suprathermal) ions generated through auxiliary heating and fusion born alpha particles remain confined until they transfer their energy to the plasma. Electromagnetic field perturbations generated by the presence of instabilities in the plasma can lead to a premature loss of the fast alphas, either through resonant or non-resonant wave-particle interaction processes [2, 3]. In tokamaks one such instability are fishbone oscillations [4, 5]. Resonant fishbone losses are not considered to be a source of concern for burning plasmas because they are predicted to involve only relatively low energy (few hundred keV) alphas [6]. However, in [6] it was also pointed out that non-resonant losses of fusion products by fishbones may become an issue, as they could affect the higher energy part of the fast alpha population. These fast ion losses are predicted to arise due to the loss of toroidal symmetry of the magnetic field configuration in the presence of the mode. Indeed, increased fusion product losses in the MeV range have been reported on a number of machines in the presence of fishbones, including JET [7–10]. In the case of [10], the losses were characterised with the help a 2-D scintillator diagnostic for lost ions [11], shown in figure 1, assessing in particular the energy and pitch angle distribution of the losses, their scaling with the fishbone amplitude as well as the losses' temporal evolution during a fishbone cycle. Also in [10], results from numerical simulations were presented which, using a number of simplifying assumptions, aimed at reproducing the experimental measurements. The simulation results were mostly in broad agreement with experiment, but some of the predictions could not be reconciled with experiment using this model. This article is a continuation of that work. Compared to [10], an improved numerical model has been used through the development of a synthetic diagnostic model for the scintillator probe which has been incorporated into the HAGIS (v10.04) orbit following code and replicates better the actual working principle of the diagnostic. The paper is structured as follows. Section presents the numerical model used, with emphasis on the synthetic diagnostic module which replicates the scintillator probe inside HAGIS. In section this model is applied to a test case discharge and the outcome compared with experiment. In the final section a summary of results is provided, the conclusions are drawn and an outlook for future work is given.

NUMERICAL MODEL

A time dependent 3-D magnetic configuration is constructed by superimposing the perturbation field of an internal kink mode (whose radial eigenfunction is a good approximation for the fishbone) to the axisymmetric equilibrium. Here, the radial eigenfunctions are computed by the linear MHD code MISHKA-1, which solves the ideal incompressible MHD equations. To reproduce a typical fishbone cycle, the obtained eigenfunctions are scaled analytically with a time dependent amplitude and rotation frequency [12]. The amplitude is specified through a third order polynomial as follows. For $t \leq t_{\rm sat}$:

$$\frac{A(t)}{A_{\rm sat}} = \frac{t^2}{t_{\rm sat}^3}\left(3t_{\rm sat} - 2t\right) \tag{1}$$

whereas for $t_{\rm sat} < t \leq t_{period}$:

$$\frac{A(t)}{A_{\rm sat}} = \left(t_{\rm period} - t\right)^2 \frac{\left[3\left(t_{\rm period} - t_{\rm sat}\right) - 2\left(t_{\rm period} - t\right)\right]}{\left(t_{\rm period} - t_{\rm sat}\right)^3} \tag{2}$$

where $A \equiv \delta\tilde{B}_r/B_0$ is the radial perturbation amplitude (normalised to the magnetic field on axis), $t_{\rm sat}$ is the time at which the maximum fishbone amplitude, $A_{\rm sat}$, is reached, and $t_{\rm period}$ is the total duration of the fishbone. The waveform appearance is illustrated in figure 2. The perturbation frequency is chosen to decrease linearly in time over the fishbone period.

The drift-orbit following code HAGIS [13, 14] follows an ensemble of fast particles in the time dependent magnetic field configuration throughout the duration of a fishbone cycle, where the initial fast particle ensemble is computed externally by a Fokker-Planck Monte Carlo solver (for the example presented in section this code is SELFO). In order to simulate the scintillator probe measurements, a synthetic diagnostic model has been added to HAGIS, whose layout is shown in figure 3. Each time a guiding center crosses a pre-defined horizontal plane $Z = Z_{\rm probe}$, HAGIS computes the ion's Larmor radius and checks by how much the guiding center distance to the probe entrance slit (centered at $R_{\rm probe}$, $Z_{\rm probe}$) deviates from the Larmor radius. If this deviation is less than a given tolerance value (this value determines the effective radial width of the probe slit in the simulation), the ion is pre-selected. In reality, the actual width of the probe slit is 0.6 mm, but the tolerance value used here was set to 1 cm in order to improve the simulation statistics. For the same reason, in the model the probe slit is chosen to be not toroidally localised (so we assume toroidal symmetry of the losses), whereas in reality the toroidal extension of the probe slit is a few mm only. Furthermore, it is ensured that each ion can be detected only once (recurrent detections are ignored). In practice some of the ions would have been detected also in the absence of a perturbation. These ions are discarded through comparison with a reference simulation for which the perturbation field has been switched off. The collimator of the real scintillator probe is designed in such a way that only ions whose gyroradius and pitch angle lie within a certain range (3-13 cm and 35-85 degrees, respectively), can actually hit the scintillator plate, so ions which fall outside this range are discarded in the synthetic diagnostic. For a successful detection the ions also need to be reaching the slit within an allowable range of gyrophases (the incidence angle must not deviate

by more than approximately 25 degrees from the slit plane normal). This is ensured by requesting that the guiding center does not deviate by more than $\Delta Z/2$ from $Z_{\rm probe}$ for detection (shaded area in figure 3). In practice, ΔZ is not an explicit parameter, but its value has been fixed indirectly by adjusting the numerical stepsize when computing the orbit trajectory. Here, the value of $\Delta Z/2$ was approximately 1 cm. An important approximation that had to be made concerns the probe location. As for the discharge analysed here the actual probe entrance is away from the plasma boundary by more than a gyroradius, and since with the HAGIS version available for our studies it was not possible to compute orbit trajectories outside the separatrix, it became necessary to shift the probe position radially inwards by 7 cm. The impact of this artificial shift on the simulation results will be assessed later. It is finally noted that this geometric description is different to the one used previously in [10] (there, the criterium used for selection was that particles had to cross the separatrix within a range of poloidal angles in the vicinity of the probe, $0^o \leq \theta \leq 60^o$), and that the new model replicates better the actual working principle of the scintillator diagnostic.

APPLICATION TO JET DISCHARGE

We have repeated an earlier analysis done for JET discharge 69100, documented in detail in [10], with the improved numerical model. A brief review of the discharge characteristics and main experimental findings is given here for convenience.

Discharge 69100 is an ELMy H-mode discharge with conventional (fully relaxed) q-profile. During its flat top ($t = 21.0 - 23.4$ s) the discharge parameters are as follows: $B_0 = 2.7$ T, $I_p = 1.2$ MA, edge safety factor $q_{95} \sim 6.5$, normalised beta $\beta_{\rm N} = 2.6$, poloidal beta $\beta_{\rm pol} = 1.8$, Greenwald fraction $n_e/n_{\rm GW} = 0.77$, triangularity $\delta \sim 0.4$. The plasma is composed of 95 percent deuterium and 5 percent hydrogen (inferred from visible spectroscopy measurements at the plasma boundary). The auxiliary heating consists of 15 MW of NBI (deuterium, max. 130 keV injection energy) and 6 MW of coupled ICRH (42 MHz, giving for the hydrogen minority a central resonance position 28 cm inboard of the magnetic axis). The neutral particle analyser (NPA) diagnostics show negligible second harmonic deuterium acceleration, which is in agreement with PION [15] and SELFO [16] simulations. Fishbone bursts are repeatedly observed throughout the flat-top phase. Their occurrence is accompanied by a temporary increase in fast ion losses detected by the scintillator probe (figure 4). Neutron emission traces and also ICRH-free reference discharges demonstrate that the fishbones are driven unstable by neutral beam injected deuterons. However, any neutral beam deuterons lost from the plasma (e.g. due to resonant interaction with the fishbone wave field) will not be detected by the scintillator diagnostic as deuterons with $E_{\rm D} < 200$ keV are blocked by a gold foil with 1 μm thickness mounted at the probe entrance. Instead, the fast ion losses seen on the scintillator probe are identified as ICRH-accelerated protons in the megaelectronvolt energy range, which become lost due to non-resonant wave-particle interaction [10].

For the simulations, the proton distribution of ICRH-accelerated protons in the plasma has been computed with the SELFO code for this discharge. The resulting distribution has been validated

against NPA measurements by comparing the perpendicular tail temperature (mean energy in the perpendicular degrees of freedom) of the simulated distribution along the NPA's line of sight with the actual NPA measurement. Within the measurement uncertainty, excellent agreement is found between the two tail temperatures (249 keV by SELFO, 240 $\pm$ 65 keV by NPA).

The magnetic perturbation field computed by MISHKA (internal kink mode including poloidal harmonics $-2 \leq m \leq +4$) is superimposed to the 2D equilibrium using the following parameters: $t_{\rm sat} = 1.8$ ms, $t_{\rm period} = 11.0$ ms, $f_{\rm start} = 7$ kHz, $f_{\rm end} = 2$ kHz, whereas $A_{\rm sat}$ has been varied between $0.25 - 1.50 \times 10^{-2}$ to cover the full range of fishbone amplitude values observed in discharge 69100. Here, the first two parameters have been inferred directly from magnetic fluctuation traces, the third and fourth parameters are the fishbone fluctuation frequencies after deduction of the core plasma rotation near the $q = 1$ rational surface (from charge exchange recombination spectroscopy). Finally, the value of $A_{\rm sat} = \delta\tilde{B}_{r,\rm sat}/B_0$ has been obtained by matching the magnitude of magnetic flux surface displacements inside $q = 1$ (visualized through Poincare plots of magnetic field lines in the 3-D perturbed equilibrium) to electron temperature profile displacements at the time of maximum fishbone amplitude measured with an array of ECE radiometers. The electron temperature profile displacements are in turn obtained using the expression

$$\xi = \frac{\delta T_e}{|\nabla T_e|} \tag{3}$$

which neglects plasma compressibility [17]. It is noted that the distortion of the total magnetic field (ECE measurement position) as a result of the fishbone perturbation is negligible, and that the plasma is optically thick at the location of interest, so the ECE signal responds indeed only to electron temperature variations.

The simulation results are as follows. As in the earlier simulations (cf also [10], figures 12 and 13), two orbit types are the main contributors to the detected losses: (a) trapped protons whose outer orbit leg runs close to the plasma boundary (and thus were already passing by in the vicinity of scintillator diagnostic), and (b) from counter-passing protons deep inside the plasma which transit into a trapped orbit similar to (a). In both cases the orbit distortions are found to originate from non-resonant wave particle interaction. Figure 5 compares the measured and simulated energy distributions of lost protons for one of the fishbones in figure 4. It can be seen that the agreement between the two is excellent. The simulated losses follow closely the measured curve almost over the entire energy range. Only at the highest energies ($\sim$3 MeV) the losses are somewhat underestimated. Compared to the old simulation results, for which good agreement was only found if the core losses were artificially omitted, this constitutes a major improvement. The earlier results suggested that the core losses were being overestimated, but those have in fact not diminished in the new model. Hence, the improvement must come from the more accurate geometrical treatment for the losses selection.

The analogous comparison for the distribution of detected protons as a function of the pitch angle related orbit invariant $\Lambda = \mu_m B_0/E = B_0(1 - \cos^2\vartheta_p)/B$ (where μ_m is the magnetic moment, E

is the proton energy, B_0 and B are the magnetic field on axis and at the probe location, respectively, and ϑ_p is the pitch angle) is shown in figure 6a. The plot includes in addition the initial SELFO distribution of protons in the plasma. Once more, the agreement between the measured and the detected losses distribution is excellent. Not only have the simulated losses the right shape (except for the regions far away from the maxima, where HAGIS underestimates the losses), but even the slight shift ($\Delta\Lambda \approx 0.08$) seen on the measured losses towards lower Λ values when comparing with the distribution inside the plasma can be reproduced. At this point, however, it is important to remember that the synthetic diagnostic position had been artificially shifted by a few cm towards the plasma. To assess the shift's impact, separate runs were performed in which the position of the probe was scanned radially, moving it further towards the plasma in small steps of about 2 cm. It turns out that while for the other results shown in this article (e.g. the energy distribution) the probe position adjustments have a negligible effect on the predictions, for the pitch angle distribution it is not negligible. What is observed is that the detected losses distribution remains Gaussian-like, but its shift with respect to the initial proton distribution varies. This is further illustrated in figure 6b, where the position of the Gaussian peak is plotted against R_{probe}. The trend is that the further outboard the probe is, the bigger the shift. Linearly extrapolating the simulation results to $R_{\mathrm{probe}} = 3.821$ m, we obtain a good match with the actually measured value (square), to within $\Lambda = 0.01$. Overall, it is concluded that both for the energy and the pitch angle distributions, the simulations are in very good agreement with experiment.

A comparison of measured and predicted proton losses per fishbone as a function of the fishbone amplitude parameter A_{sat} is shown in figure 7. The experimental data in this plot was obtained from a sample of 26 fishbones in discharge 69100 ($t = 22.170 - 23.110$ s), for which the obtained amplitudes range from $0.3 - 1.2 \cdot 10^{-2}$. A polynomial fit to the experimental data with linear and quadratic components yields essentially a purely quadratic increase of the losses with amplitude over the entire amplitude range. For the simulation data, a quadratic dependence of the losses is found as well at amplitudes $\delta\tilde{B}_{r,\max}/B_0 \gtrsim 0.75 \cdot 10^{-2}$. However, for $\delta\tilde{B}_{r,\max}/B_0 \lesssim 0.75 \cdot 10^{-2}$ the simulations predict a linear dependence (highlighted by the dash-dotted line) which is not corroborated by the experiment. The change from linear to quadratic losses with increasing mode amplitude can be understood in terms of a transition from near-boundary losses to stochastic (diffusive) losses, as described in [18] (see also [13] and [19]), but keeping in mind that the wave-particle interaction is here non-resonant. The amplitude behaviour shown in figure 7a is essentially the same as the one reported with the previous model [10] (the only difference being that the absolute number of detected losses predicted by HAGIS has now increased by about a factor 4; for this comparison, however, the absolute level of losses is unimportant as the scintillator diagnostic is not absolutely calibrated and the experimental data in figure 7 is scaled in a.u.). It has been argued in [10] that a mismatch between the simulated and the experimentally inferred values of A_{sat}, e.g. through neglecting the parallel plasma compressibility, is unlikely to be the cause for this discrepancy.

Another unresolved discrepancy that persists despite the model improvement and that we mention here for completeness is related to the temporal evolution of losses during a fishbone cycle. As had been reported in [10] (figure 14), the simulated losses peak before $t = t_{\mathrm{sat}}$, i.e. before the maximum magnetic perturbation is reached, whereas experimentally the scintillator signal tends to peak at the time when, or slightly after, the maximum magnetic perturbation is reached. Clearly, despite now being able to predict correctly the energy and pitch angle spectra of the losses, the improved geometrical treatment has not been able to resolve these latter discrepancies, pointing towards a deeper physics element which is still missing in the simulation codes, or, alternatively, to an unidentified hardware source. For the latter, one possible candidate would be the scintillator material itself (P56, or Y_2O_3:Eu^{3+}), which has a relatively long phosphorescence decay time of 2 ms. This may lead to distortions of the overall light output behaviour for fast events which however wouldn't show up on the energy and pitch angle distribution measurements [20, 21]. Efforts are underway to install a new faster scintillator material (TG-Green, or $SrGa_2S_4$:Eu^{2+}), previously deployed on ASDEX Upgrade [22, 23], which should yield further clarification.

SUMMARY AND CONCLUSIONS

A model for the simulation of pitch angle and energy resolved fast ion loss measurements from a 2D scintillator probe has been presented and successfully tested against fishbones on JET. The improved geometrical description of scintillator probe measurements through the implementation of a synthetic diagnostic module in HAGIS has proven to be key to the correct reproduction of the two primary deliverables of the diagnostic, namely the energy and the pitch angle distribution of losses. Lacking an absolute calibration of the diagnostic, we have not attempted to compare the absolute number of losses, but at least their relative variation with the fishbone amplitude has been assessed, yielding more subtle differences between experiment and simulation for lower amplitude modes (i.e. quadratic versus linear increase with fishbone amplitude, respectively) which will require further investigation.

One of the limitations encountered (which could only be overcome through a small shift of the synthetic probe location towards the plasma boundary) was the inability to trace guiding centers beyond the separatrix. In the future, this could be overcome with the help of a recent extension to HAGIS by Bruedgam $et\ al$ [24], which has been tested on ASDEX Upgrade but has still to be implemented for JET.

With only minor modifications this simulation technique can be applied to the study of other, more complex, instabilities, such as Alfven Eigenmodes or Alfven Cascades, against scintillator probe measurements. Dedicated JET experiments have been recently performed to study the influence of these instabilities on the fast ion confinement deterioration and loss [25], which are envisaged for future work.

ACKNOWLEDGMENTS

This work, supported by the European Communities under the contract of Association between EURATOM and Max-Planck Institut für Plasmaphysik, was carried out within the framework of the European Fusion Development Agreement. The views and opinions expressed herein do not necessarily reflect those of the European Commission.

REFERENCES

REFERENCES

[1] R. B. White et al. *Phys. Plasmas*, 2:2871, 1995.

[2] W. W. Heidbrink and G. J. Sadler. *Nucl. Fusion*, 34:535, 1994.

[3] A. Fasoli et al. Progress in the iter physics basis chapter 5: Physics of energetic ions. *Nucl. Fusion*, 47:S264, 2007.

[4] K. McGuire et al. *Phys. Rev. Lett.*, 50:891, 1983.

[5] L. Chen, R. B. White, and M. N. Rosenbluth. *Phys. Rev. Lett.*, 52:1122, 1984.

[6] B. Coppi and F. Porcelli. *Fusion Technology*, 13:447, 1988.

[7] W. W. Heidbrink, R. Hay, and J. D. Strachan. *Phys. Rev. Lett.*, 53:1905, 1984.

[8] H. H. Duong and W. W. Heidbrink. *Nucl. Fusion*, 33:211, 1993.

[9] S. J. Zweben et al. *Nucl. Fusion*, 30:1551, 1990.

[10] C. Perez von Thun et al. *Nucl. Fusion*, 50:084009, 2010.

[11] S. Baeumel et al. *Rev. Scient. Instr.*, 75:3563, 2004.

[12] S. D. Pinches et al. presented at 11th iaea technical meeting on energetic particles in magnetic confinement systems, 21st-23rd september 2009, kyiv. 2009.

[13] L. C. Appel et al. *Nucl. Fusion*, 35:1697, 1995.

[14] S. D. Pinches et al. *Comp. Phys. Comm.*, 111:133, 1998.

[15] L.-G. Eriksson, T. Hellsten, and U. Willén. *Nucl. Fusion*, 33:1037, 1993.

[16] J. Hedin, T. Hellsten, L.-G. Eriksson, and T. Johnson. *Nuclear Fusion*, 42:527, 2002.

[17] C. Z. Cheng. *Phys. Rep.*, 211:1, 1992.

[18] C. T. Hsu and D. J. Sigmar. *Phys. Fluids B*, 4:1492, 1992.

[19] M. García-Muñoz et al. *Phys. Rev. Lett.*, 104:185002, 2010.

[20] M. Tuszewski and S. J. Zweben. *Rev. Scient. Instr.*, 63:4542, 1992.

[21] M. Tuszewski and S. J. Zweben. *Rev. Scient. Instr.*, 64:2459, 1993.

[22] M. García-Muñoz et al. *Rev. Scient. Instr.*, 80:053503, 2009.

[23] M. García-Muñoz et al. *Phys. Rev. Lett.*, 100:055005, 2008.

[24] M. Bruedgam. *PhD thesis 2010, IPP-Garching*.

[25] V. G. Kiptily et al. *Nucl. Fusion*, 49:065030, 2009.

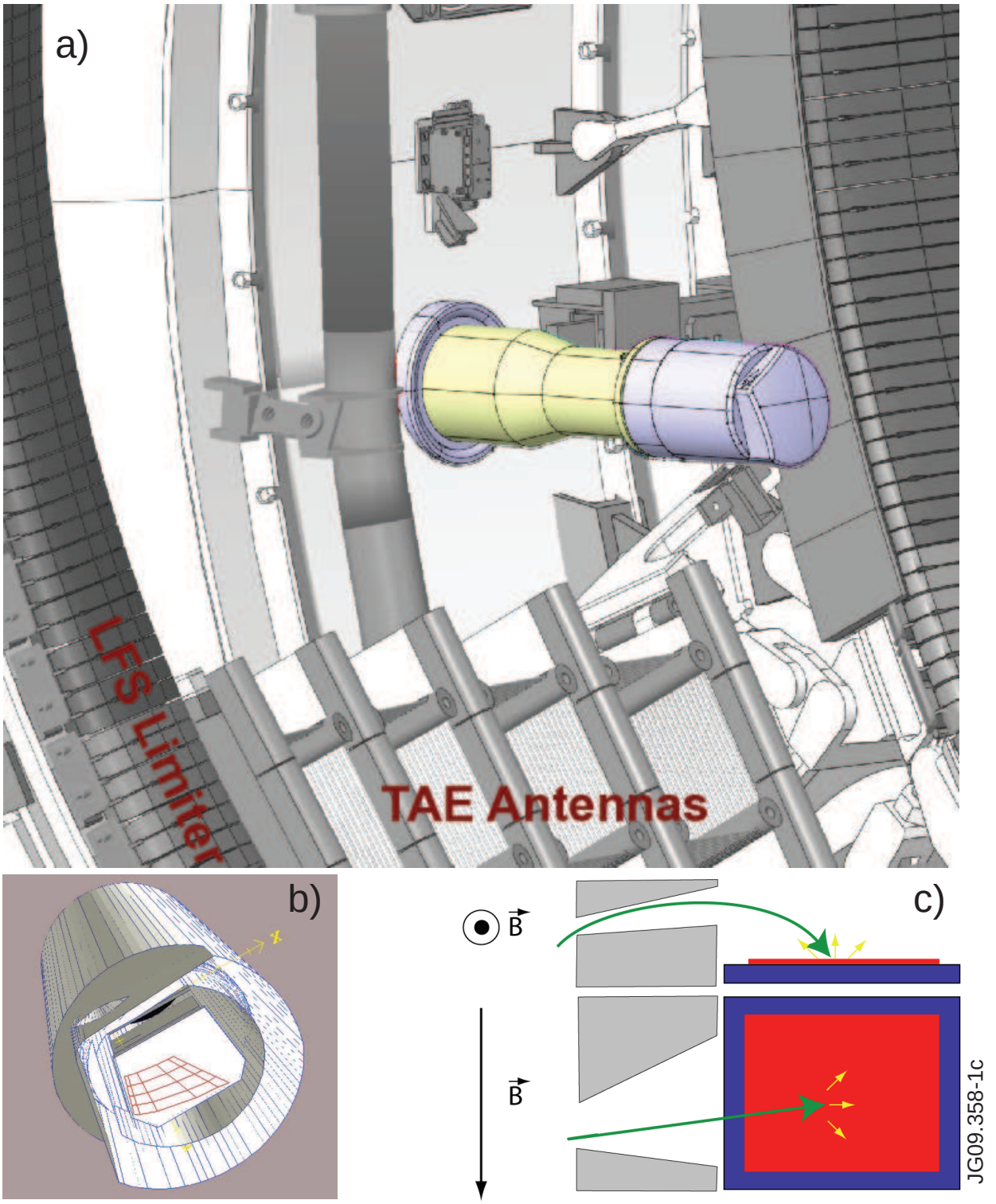

Figure 1: (a) Scintillator probe layout inside the JET vessel. (b) Cross-cut through the probe head showing the collimator and the 2-D scintillator plate. (c) Measuring principle: The location at which incoming ions hit the scintillator depends on the gyroradius and the pitchangle of the velocity vector with respect to the local magnetic field.

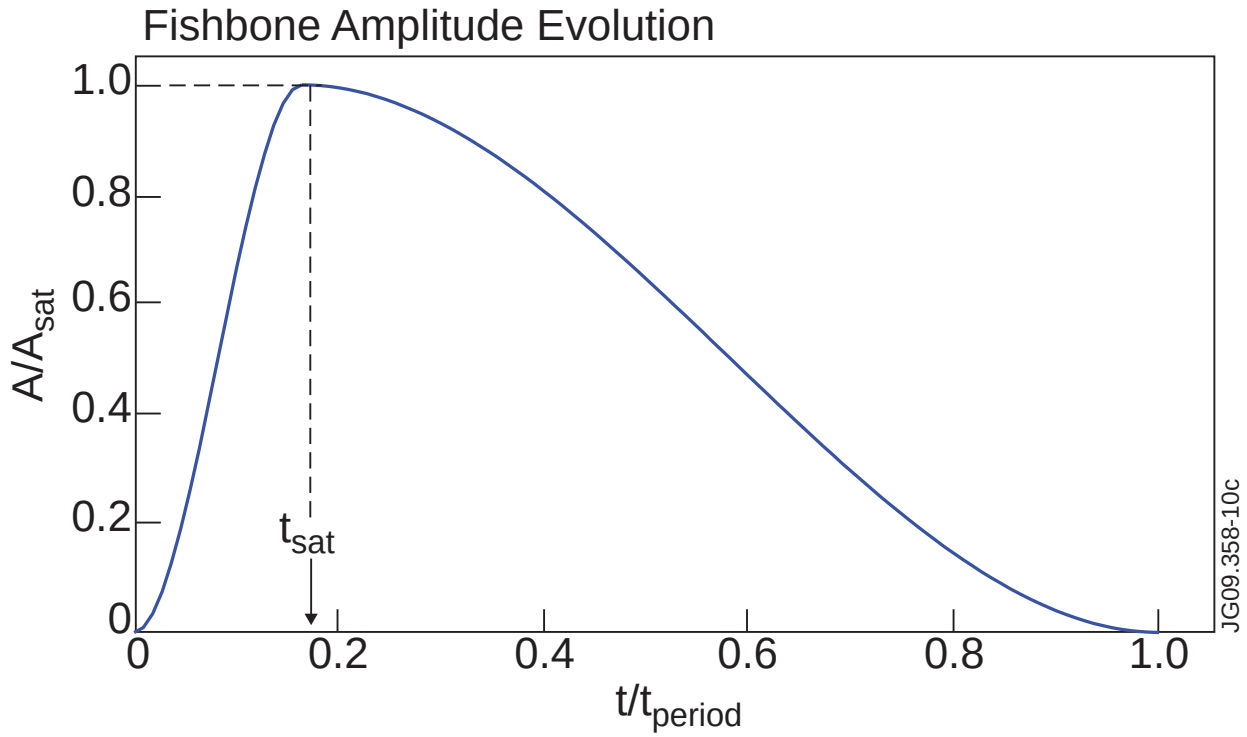

Figure 2: Waveform of the $n = 1$ kink amplitude used in HAGIS, including the definitions of the quantities t_{sat}, t_{period} and A_{sat}. $A \equiv \delta\tilde{B}_r/B_0$ is the perturbed radial magnetic field normalised to the magnetic field on axis .

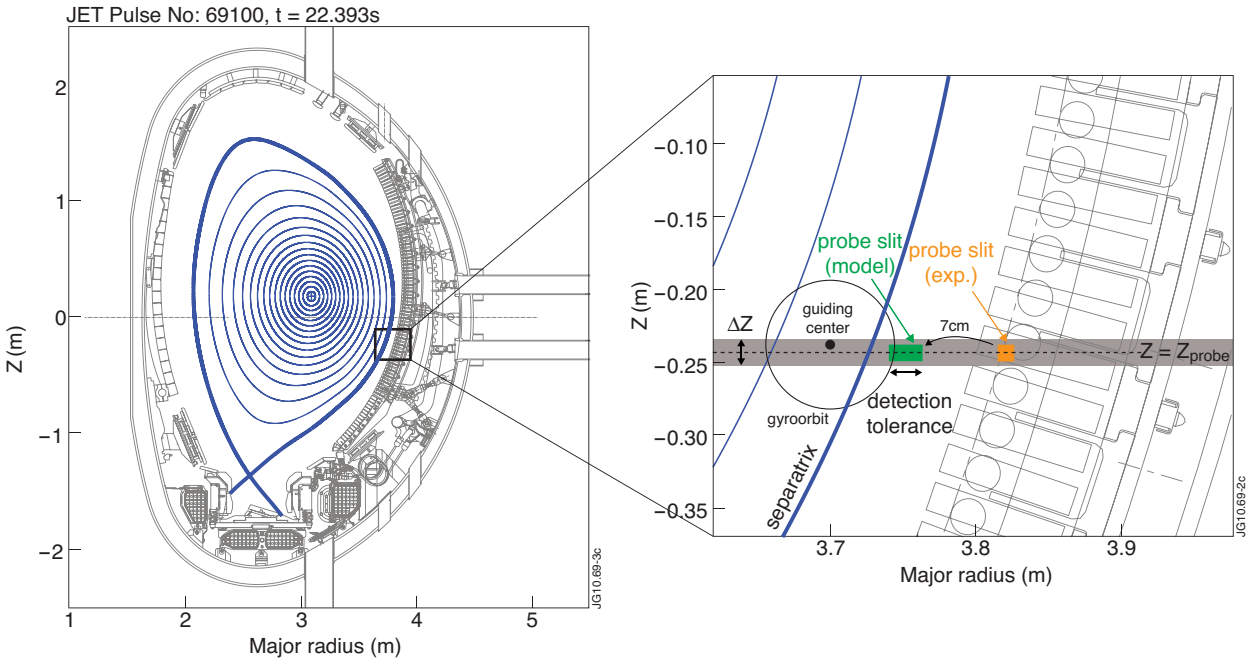

Figure 3: Synthetic diagnostic model used in HAGIS to select scintillator probe detected ions.

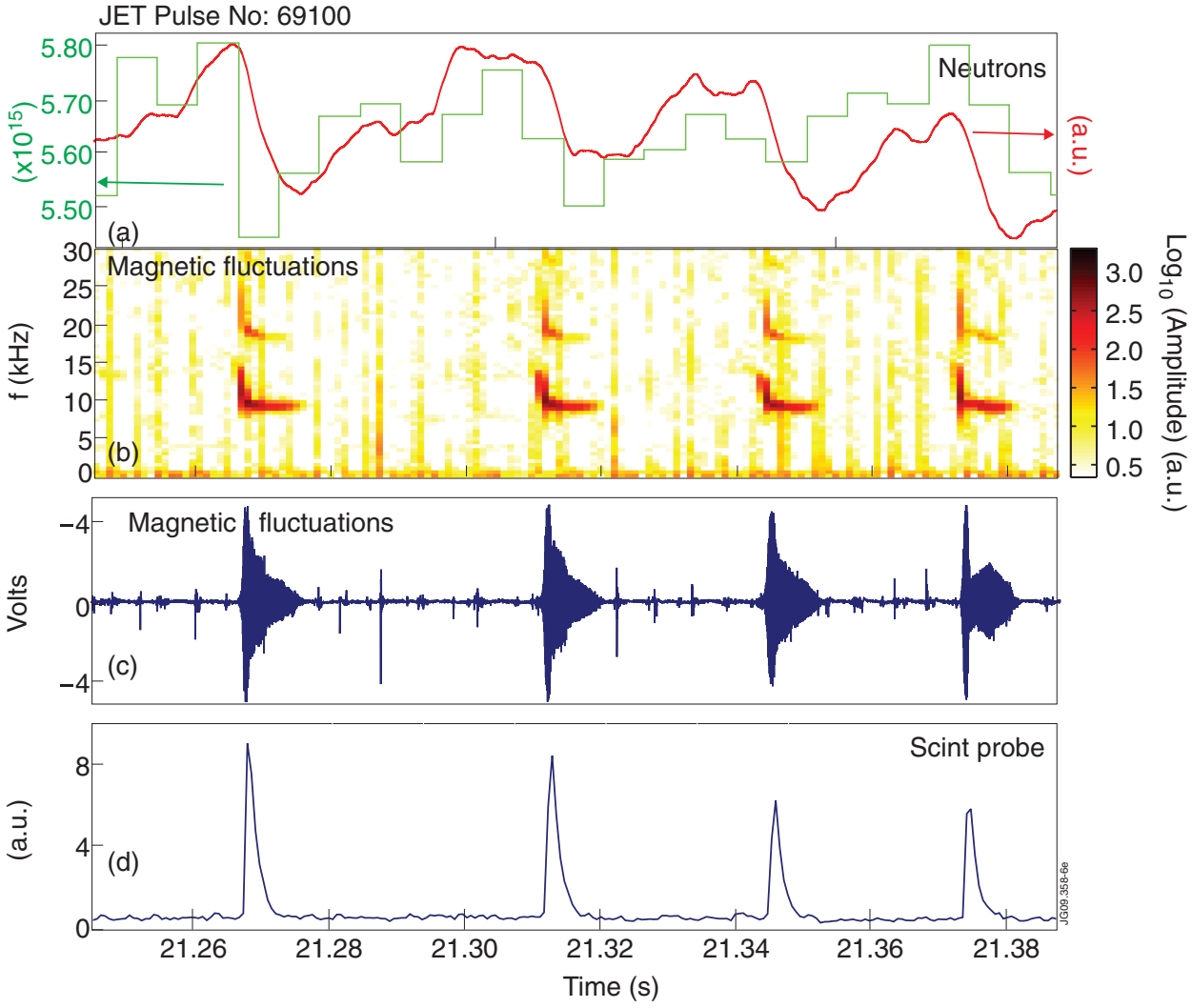

Figure 4: Time interval of discharge 69100 with four fishbones. (a): Neutron emission (two traces are shown: are a slow calibrated signal and a faster signal which is uncalibrated), (b): magnetic fluctuation spectrogram, (c): magnetic fluctuation time trace (the much smaller bursts visible on this trace are due to ELMs), (d): scintillator probe signal.

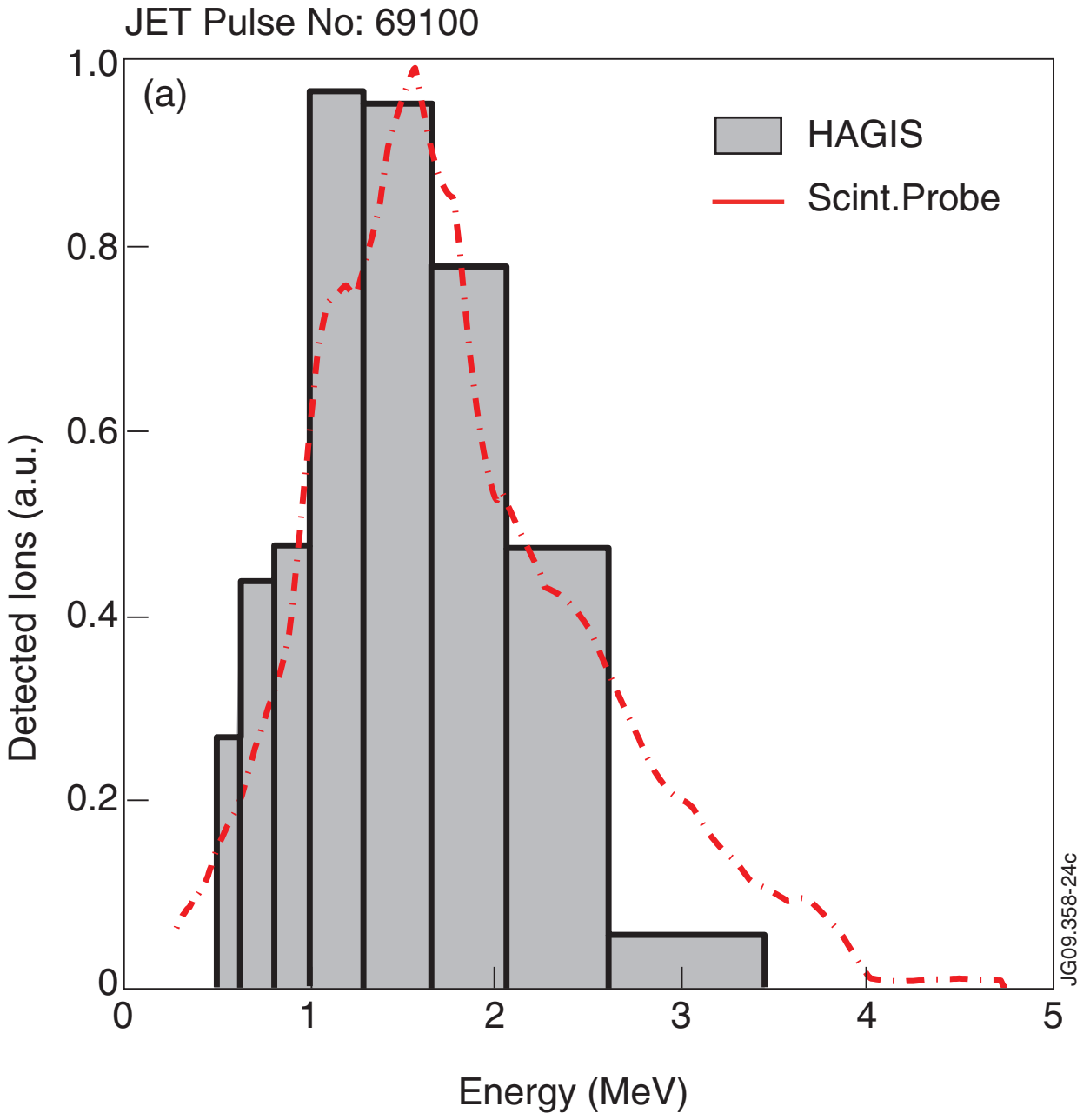

Figure 5: Energy distribution of losses measured by the scintillator probe diagnostic for the first fishbone shown in figure 4, for which a saturation amplitude value $A_{\mathrm{sat}} = 0.96 \times 10^{-2}$ (with 20-30% uncertainty) has been inferred from ECE measurements, and simulated energy distribution from HAGIS ($A_{\mathrm{sat}} = 1.0 \times 10^{-2}$) using the synthetic diagnostic module. The varying width of the energy bins for the hagis data matches the measurement uncertainty for the lost ion energy (the energy resolution of the actual scintillator probe decreases with increasing energy, whereas the pitch angle resolution does not vary). To keep the normalisation (area of bars relative to each other) correct, the number of markers falling into each energy bin is divided by the width of that energy bin. The integral over all the bars equals the integral of the measured curve.

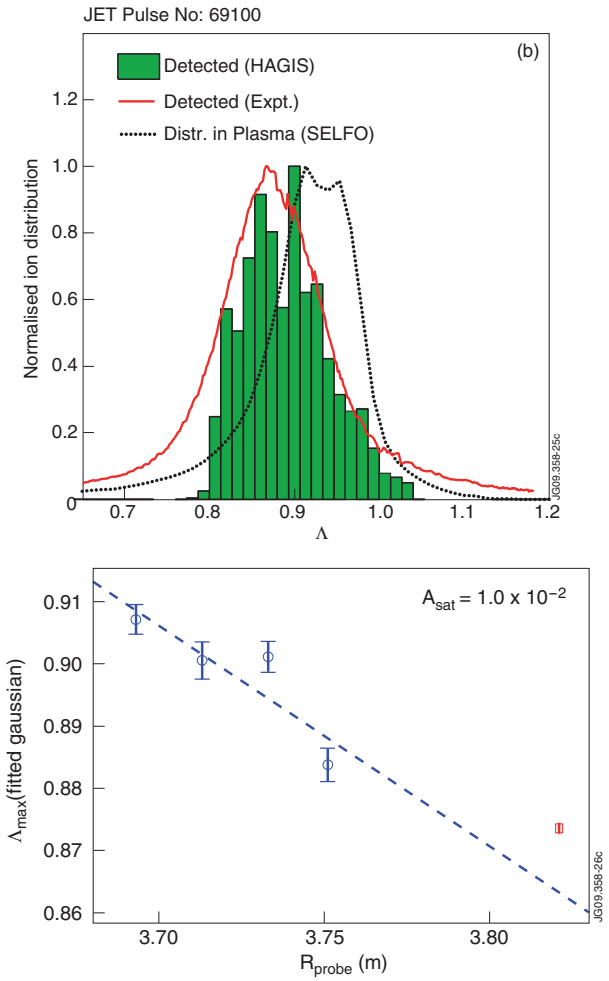

Figure 6: (a) Distribution of proton losses measured by the scintillator probe diagnostic ($R = 3.821$ m) as a function of the pitch-angle related parameter $\Lambda = \mu_m B_0/E$ for the same fishbone as in figure 5, and distribution predicted by HAGIS using the synthetic diagnostic module. Here, the synthetic diagnostic is located at $R = 3.751$ m. Also shown is the Λ distribution of the total fast proton population inside the plasma. Note that all three distributions are here normalised to their respective maxima (only a tiny fraction of the original proton population in the plasma reaches the detector). The measured losses distribution (solid curve) peaks at $\Lambda = 0.874$, which corresponds to a pitch angle of 58.0^o. A Gaussian fitted to the SELFO distribution (dotted curve) peaks at $\Lambda = 0.926$, which corresponds to a pitch angle of 61.0^o. (b) Influence of the synthetic diagnostic radial position on the predicted Λ distribution. The y-axis denotes the Λ value at which a Gaussian function fitted to the simulated losses has its maximum. The circles are obtained from the simulations, whereas the square is the actual measurement (fitted Gaussian to the solid curve in (a)). The error bars give the 95% confidence bounds of the fit. The linearly extrapolated value of the position of the Gaussian maximum predicted by the simulations for $R = 3.821$ m is in fairly good agreement (to within $\Lambda = 0.01$ or, equivalently, 0.5^o in pitch angle) with the measurement.

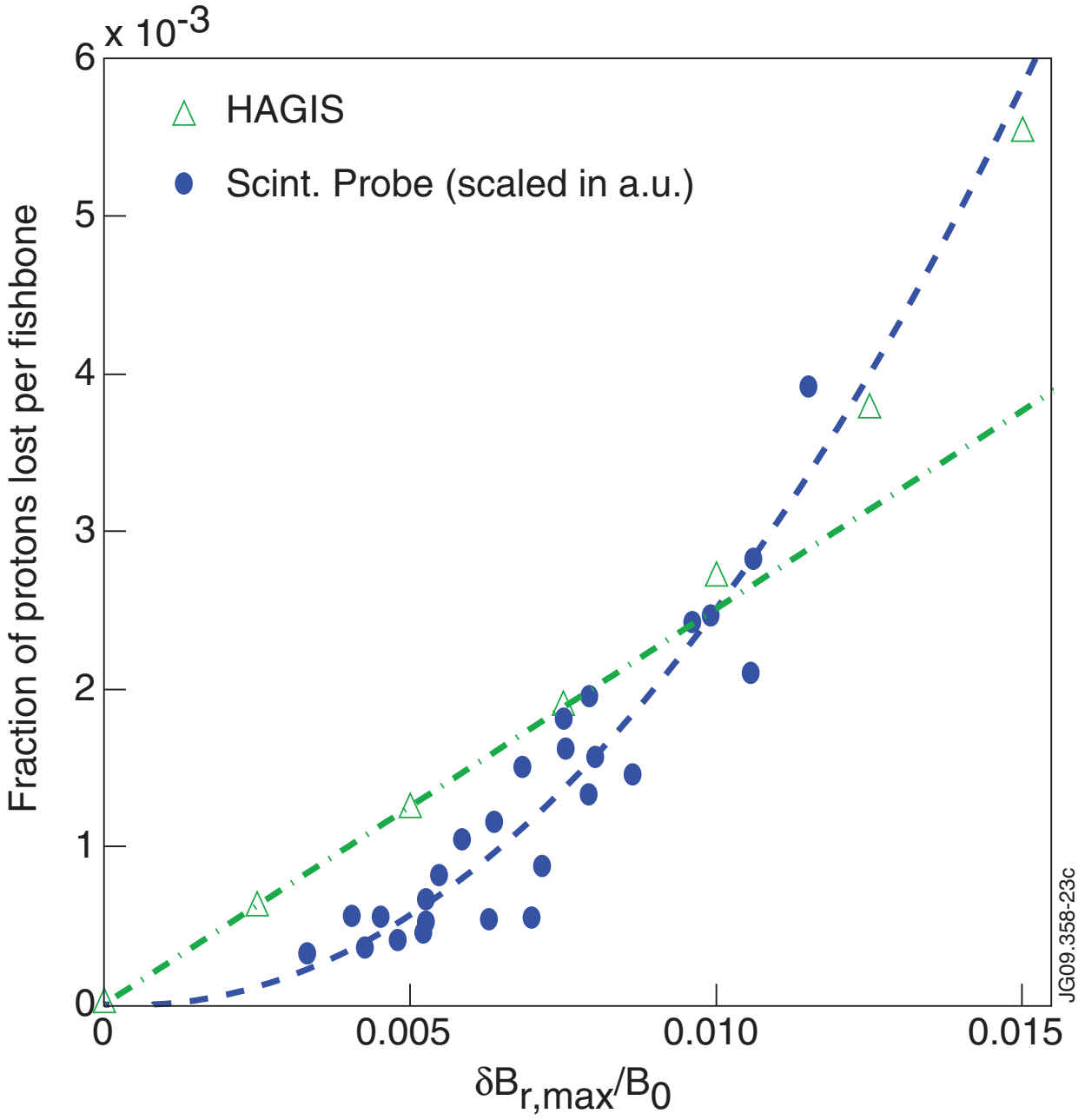

Figure 7: Measured (circles) and simulated (triangles) losses dependence on the fishbone amplitude parameter $A_{\rm sat} = \delta B_{r,\max}/B_0$. *For the experimental data, the value of* $A_{\rm sat}$ *has been obtained by matching the magnitude of magnetic flux surface displacements inside* $q = 1$ *(visualized through Poincare plots of magnetic field lines in the 3-D perturbed equilibrium) to electron temperature profile displacements at the time of maximum fishbone amplitude measured with an array of ECE radiometers.*